applied sciences

IMPACT FACTOR 2.7

CITESCORE 4.5

Article

# Raman Spectroscopy to Monitor the Delivery of a Nano-Formulation of Vismodegib in the Skin

Gisela Eliane Gómez, María Natalia Calienni, Silvia del Valle Alonso, Fernando Carlos Alvira and Jorge Montanari

Special Issue

Young Investigators in Advanced Drug Delivery

Edited by

Dr. Antonia Mancuso and Dr. Gianpiero Calabrese

MDPI

https://doi.org/10.3390/app13137687

applied sciences

MDPI

*Article*

# Raman Spectroscopy to Monitor the Delivery of a Nano-Formulation of Vismodegib in the Skin

**Gisela Eliane Gómez [1,2,3], María Natalia Calienni [1,2,4,5], Silvia del Valle Alonso [1,2], Fernando Carlos Alvira [1,2] and Jorge Montanari [1,2,4,5,*]**

[1] Laboratorio de Bio-Nanotecnología, Departamento de Ciencia y Tecnología, Universidad Nacional de Quilmes, Bernal 1876, Argentina; giselae.gomez@gmail.com (G.E.G.); natalia.calienni@unahur.edu.ar (M.N.C.); salonso@unq.edu.ar (S.d.V.A.); fcalvira@gmail.com (F.C.A.)
[2] Grupo de Biología Estructural y Biotecnología (GBEyB), IMBICE (CONICET CCT-La Plata), Buenos Aires 1906, Argentina
[3] Laboratorio de Patología y Farmacología Molecular, Instituto de Biología y Medicina Experimental (IBYME-CONICET), Buenos Aires 1428, Argentina
[4] Laboratorio de Nanosistemas de Aplicación Biotecnológica (LANSAB), Universidad Nacional de Hurlingham, Av. Vergara 2222, Villa Tesei, Buenos Aires 1688, Argentina
[5] Comisión de Investigaciones Científicas de la Provincia de Buenos Aires (CIC), La Plata 1900, Argentina
* Correspondence: jorge.montanari@unahur.edu.ar

**Featured Application: Raman spectroscopy could be used as a non-invasive and rapid detector of small molecules in the skin of patients.**

**Abstract:** Raman spectroscopy was used to detect low quantities of Vismodegib in the skin after its topical application via transfersomes. Vismodegib is a novel antineoplastic drug approved for oral administration for treatment of basal cell carcinoma. Transfersomes loaded with Vismodegib were prepared by thin film resuspension and extrusion, and were characterized physicochemically. Transfersomes were applied to human and pig skin specimens using the Saarbrücken penetration model. The skin was then sectioned by tape stripping, followed by penetration assessment by UV-Vis spectroscopy and Raman spectroscopy in a confocal Raman microscope. Raman signals from Vismodegib and transfersomes were recovered from skin sections, showing a similar distribution in the *stratum corneum* obtained by the other techniques. On the other hand, pig and human skin showed differences in their penetration profiles, proving their lack of equivalence for assessing the performance of these transfersomes. Raman spectroscopy appears as a potential non-invasive, direct tool for monitoring hard-to-detect molecules in a complex environment such as the skin.

**Keywords:** Raman spectroscopy; skin penetration; Vismodegib



**Citation:** Gómez, G.E.; Calienni, M.N.; Alonso, S.d.V.; Alvira, F.C.; Montanari, J. Raman Spectroscopy to Monitor the Delivery of a Nano-Formulation of Vismodegib in the Skin. *Appl. Sci.* **2023**, *13*, 7687. https://doi.org/10.3390/app13137687

Academic Editors: Gianpiero Calabrese and Antonia Mancuso

Received: 6 June 2023
Revised: 27 June 2023
Accepted: 27 June 2023
Published: 29 June 2023



## 1. Introduction

The epidermis, which makes up the majority of the surface of the skin, is composed of keratinocytes produced from the basal stratum and is divided into many layers. The outermost epidermal layer, known as the *stratum corneum* (SC), is made up of corneocytes that are encased in a lipid matrix. Vismodegib (VDG) (Erivedge®, Genentech) is a novel antineoplastic drug approved for its use by oral administration in basal cell carcinoma, a type of skin cancer [1]. In recent years, research has been conducted on the local administration of VDG through topical applications in order to minimize systemic distribution and mitigate potential side effects. [2,3]. Transfersomes are a special kind of unilamellar liposomes, composed of a mixture of phospholipids and an edge activator that confers deformability to their membrane, and they are among the carriers that have been proven useful to deliver VDG to the viable epidermis. Their enhanced flexibility and fluidity make them especially useful for skin delivery, as they can pass through the very narrow

channels that exist in the SC to reach the viable epidermis, where they can release their cargo [4]. In order to determine whether a compound loaded into transfersomes, or any other skin delivery system, effectively overcomes the SC barrier and reaches the viable epidermis, it is necessary to assess its distribution across these skin regions. For this purpose, *in vitro*/*ex vivo* techniques, such as Franz cell permeation studies or penetration studies using the Saarbrücken penetration model, are employed or, alternatively, in vivo incubation in animal models, which requires sacrificing the individuals prior to determination. In living human subjects, the tests can, at most, investigate the distribution within the SC, using the in vivo tape stripping technique—which causes an increase in trans epidermal water loss, is painful, and leaves the skin damaged for a period of time—without providing insight into the distribution of the compound in the layers of the viable epidermis and beyond [5].

On the other hand, Raman spectroscopy is a sensitive and non-destructive technique that involves the use of optical filters to analyze the scattered radiation and obtain information about molecular structure, relying on the emission of photons, which form the unique fingerprint of functional groups [6]. Thus, it provides not only qualitative information, but also quantitative conformational analysis [7]. It is based on inelastic scattering, and measures the change in energy of the scattered radiation. Raman scattering is considered a weak, second-order process due to the interaction of the laser photons and the vibrational mode of the sample under analysis. It is a low-damage, high-sensitivity method, which make it suitable for studying lipids and drugs [8], and its potential to detect molecules in the skin has been pointed out in the past decade [9]. Recent advancements in Raman spectroscopy have expanded its capabilities, allowing for more precise and detailed analyses of samples. The Raman spectrum of VDG was previously studied [10] through their characteristic functional groups, such as pyrimidine, amide, sulfone, phenyl, and chlorine groups. Therefore, Raman spectroscopy could be of great utility in detecting compounds loaded in drug delivery systems for topical-cutaneous administration, allowing for safe monitoring of their effective arrival to deep skin layers in living individuals. This could contribute to improved treatment monitoring and optimization of dosages, by correlating the actual amount of the compound in the skin with measured effects. To pave the way towards that aim, in this work, the Raman technique is used to determine VDG directly from human and pig skin samples.

## 2. Materials and Methods

### 2.1. Materials

Soybean phosphatidylcholine (SPC) was purchased from Avanti Polar Lipids (Alabaster, AL, USA), while sodium cholate (NaChol) and Merocyanine 540 (MC540) were purchased from Sigma-Aldrich (Buenos Aires, Argentina). Erivedge® (commercial name for VDG) tablets and VDG standard (2-chloro-N-(4-chloro-3-(pyridin-2-yl)phenyl)-4-(methylsulfonyl) benzamide) were donated by Roche S.A.Q. e I. 6-Dodecanoyl-2-dimethylaminonaphthalene (Laurdan, Birmingham, AL, USA) was obtained from Thermo Fisher Scientific (Buenos Aires, Argentina). The remaining analytical-grade reagents were obtained from Anedra (Buenos Aires, Argentina).

### 2.2. VDG Extraction from Capsules and Its Quantification

The extraction and quantification of VDG from commercially-formulated capsules were conducted according to a previously described method [11]. Briefly, the capsules' contents were extracted using methanol (1 mL of solvent per 4 mg of Erivedge®) through vortexing for 1 min, followed by centrifugation, yielding a recovery rate of 78.8 ± 7.2% in the supernatant. VDG determination was performed with a Shimadzu UV-1800 UV-Visible spectrometer, using 270 nm as absorption wavelength, and a calibration curve was generated from triplicate measurements of the standard, covering a concentration range of 0.24–24 μM ($Y = 0.019 \times X - 0.0238$; $R^2 = 0.9917$).

### 2.3. Transfersomes Obtention

Transfersomes containing VDG (T + VDG) were prepared as in previous works [12]. The liposomes were formulated using a mixture of SPC and NaChol, to which VDG dissolved in methanol was added in a ratio of 40:7:1.4 $w/w$ (SPC:NaChol:VDG). Briefly, the aforementioned mixture was combined with a chloroform: methanol solution in a 1:1 $v/v$ ratio. The solvents were then evaporated using a rotary evaporator at 120 rpm in a flask until complete removal, to obtain a lipid film at the bottom of the flask. The lipid film was subsequently hydrated with 1 mL of Tris-HCl buffer containing 0.9% $w/v$ NaCl at pH 7.4 (40 mg of SPC per ml of rehydration solution). Finally, the liposomal suspension underwent size and lamellarity reduction using an automatic extruder (Transferra, Burnaby, BC, Canada) connected to a nitrogen gas tank ($N_2$). The liposomal suspension was passed through a 100 nm pore-size polycarbonate membrane five times to achieve size reduction and uniformity, rendering unilamellar transfersomes with a diameter of about 100–120 nm. Transfersomes without VDG (T) were prepared in the same way, but without the addition of the drug.

### 2.4. Transfersomes Characterization

The Z-average was determined by dynamic light scattering (DLS) with a Malvern Zetasizer Nano (Malvern Instruments; Malvern, UK) at 25 °C, after appropriate dilutions. Each sample was analyzed three times. Zeta potential was determined with the same equipment in triplicate. The interaction of VDG with the transfersomes' membrane, and the changes in the membrane packing and fluidity after incorporation of the drug, were assessed with the MC540 and Laurdan probes in triplicate. For the measurement with MC540, samples were diluted with Tris-HCl buffer until a concentration of 172 µM of lipids, and the probe was added in a 1:200 molar ratio. The samples were incubated for 2 min, and then scans between 400 and 600 nm were obtained with a UV–Vis spectrophotometer (Jasco V-550, Tokyo, Japan) at 25 °C. The partition coefficient (PC) was calculated as the ratio of the maximum absorbance of the MC540 monomer in a non-polar phase (570 nm) with the maximum absorbance of the monomer in an aqueous phase (530 nm) [13]. A baseline correction was performed to avoid scattering measuring samples without the probe. PC was calculated by:

$$PC = A570/A530 \quad (1)$$

Laurdan was incorporated into T and T + VDG during their preparation by adding the probe to the lipophilic phase in a 0.33 mol% concentration. Samples were diluted with Tris-HCl buffer until forming a concentration of phospholipids of 80 µg/mL, and the fluorescence was measured with a FluoroMate FS2 (SCINCO, Seoul, Republic of Korea) at 25 °C. Generalized polarization (GP) spectra of Laurdan excitation (GPex) and emission (GPem) were calculated and graphed [14]. GPex spectra were calculated by:

$$GPex = (I_{440} - I_{490})/(I_{440} + I_{490}) \quad (2)$$

using excitation wavelengths from 320 to 400 nm. The $I_{440}$ and $I_{490}$ are the emission intensities at 440 and 490 nm, which correspond to the emission maxima of the probe in the gel and the liquid-crystalline phase, respectively. GPem spectra were calculated by:

$$GPem = (I_{390} - I_{340})/(I_{390} + I_{340}) \quad (3)$$

using emission wavelengths from 420 to 510 nm. The $I_{390}$ and $I_{340}$ are the excitation intensities at 390 and 340 nm, which correspond to the excitation maxima of the probe in the gel and the liquid-crystalline phase, respectively.

On the other hand, the molar ratio between the phospholipids and VDG was determined in triplicate. Phospholipids were quantified by the colorimetric method adapted from Stewart [15].

Statistical analyses were conducted with GraphPad Prism 8.0.1 (GraphPad Software Inc., San Diego, CA, USA). Data were analyzed using Student's t-test after the normal data distribution was confirmed with the Shapiro–Wilk test. The homoscedasticity was also corroborated using the F test to compare variances. Values with $p < 0.05$ were considered significant.

### 2.5. Obtention and Preparation of Skin Samples

Human skin explants from a healthy adult male donor were used in this study, obtained from surgical discard from abdominal surgery. The explants were conducted following approved protocols by the Ethics Committee of the National University of Quilmes (Resolution #CE-UNQ 001/19), in accordance with the World Medical Association's Code of Ethics. Samples were pinned from their ends onto a Styrofoam plate covered with aluminum foil. Scissors and scalpels were used to separate the adipose tissue (hypodermis) from the dermal tissue, leaving only a thin layer of skin containing the viable epidermis plus dermis (VED). Samples were then cleaned with PBS buffer pH 7, cut into rectangles, wrapped in aluminum foil, stored in airtight, polyethylene zip-lock bags to remove air, and kept at −20 °C until use.

Adult pig ears were bought from a slaughterhouse. The skin was separated from cartilage by carefully lifting it with forceps and using scissors. The obtained thin skin layers were then cleaned with PBS buffer, wrapped, stored, and kept at −20 °C, as with the human skin.

### 2.6. Skin Experiments

Human or pig skin samples with a diameter of 24 mm were excised and placed onto Teflon devices, known as the Saarbrucken Penetration Model (SPM) [12]. These devices consist of a flat-bottomed cylindrical cavity measuring 25 mm in diameter and 5 mm in depth. Prior to placement, a filter paper disk soaked in 200 µL of PBS was positioned on the cavity floor to create a highly humid environment, replicating the moisture gradient across the *stratum corneum* (SC). Each skin disk was evenly distributed with 20 aliquots of 2.5 µL (totaling 50 µL) of T + VDG suspension and incubated at 33 °C for 1 h. All experiments were conducted in quadruplicate. Subsequently, the skin was affixed to a polystyrene plate using pins, and *tape stripping* was performed using 20 consecutive adhesive tapes loaded with a weight of 2 kg for 10 s, after which they were rapidly removed, taking along a layer of the SC.

For the spectrometry assays, the tapes from each sample of human or pig skin were grouped into tubes corresponding to the shallow (tapes 1–5), middle (6–10), and deep (11–20) SC regions. Additionally, the remaining skin disk, consisting of viable epidermis and dermis (referred to as VED), was mechanically disrupted, and placed in an extra tube. Then, the samples were extracted for 1 h under stirring, using the same solvent used for the calibration curve, followed by the determination of the presence of VDG in each sample as in Section 2.2.

For the Raman assays, representative adhesive tapes (0.04 mm) of the different human and pig skin portions (tapes number 1, 9, and 15 from the SC, as well as the intact portion of VED with a thickness of 3.62 mm and 3.15 mm for human and pig, respectively), were collected from each sample. The tapes were lifted using tweezers and stretched over a microscope slide, securing them in a manner that the adhesive surface which was in contact with the SC faced upwards. A *Horiba Yovin Ivon* confocal Raman microscope (Horiba Ltd., Kyoto, Japan), equipped with a 785 nm laser emitting at a maximum power of 150 mW, was utilized to analyze the VDG signal. The system is equipped with an objective of 20×, with a working distance of 1.2 mm, an effective focal length of 0.9 mm, and a numerical aperture of 0.4. This objective has a focal volume of 0.2 $mm^3$.The microscope employed a *Cross Czerny Turner* spectrometer, with a grating of 600 lines/mm as its detector, with an optical resolution of 1 $cm^{-1}$. The detector in this monochromator was a CCD cooled to −60 °C. The obtained data were subsequently processed using Labspec software

10.4 (Dilor) to generate Raman spectra. The entire thickness of the sample could not be completely estimated, due to limitations of the equipment.

Blanks of untreated skin were prepared and subjected to the same procedures, to determine whether the skin or the adhesive tape generate Raman or UV-Visible signals that could act as interferences for the spectra of interest. Empty transfersomes were also used as another control.

## 3. Results and Discussion

### 3.1. Transfersomes Characterization

The loading of VDG did not alter the Z-average nor the zeta potential of the transfersomes (Table 1). Both formulations presented a unimodal distribution of size and a polydispersity index (PDI) < 0.100. The final molar ratio between VDG and lipids was 1:12.5.

**Table 1.** Physicochemical parameters of the empty and VDG-loaded transfersomes.

| Sample | Z-Average (nm) [a] | Zeta Potential (mV) [a] | Molar Ratio (VDG:SPC) | MC540 CP (A570/A530) [a] |
|---|---|---|---|---|
| T | 111.0 ± 1.8 | −20.3 ± 1.2 | - | 0.94 ± 0.01 |
| T + VDG | 114.3 ± 1.1 | −18.5 ± 0.8 | 1:12.5 | 1.00 ± 0.01 |

[a] Mean ± SD ($n$ = 3).

Since VDG is a lipophilic drug, it inserts into the transfersome phospholipid bilayer. A MC540 probe is useful to assess the phospholipid packing in bilayers by measuring its partition as a monomer between polar and non-polar environments [16], the external aqueous phase, and the transfersome's membrane, respectively. The MC540 locates as a monomer slightly above the domain of the glycerol of the backbone of neutral and charged phospholipids [17]. For this reason, MC540 is sensitive to structural variations in the head group region. The loading of VDG into the transfersomes did alter the PC of MC540 (** $p < 0.002$), increasing the PC value with respect to the empty transfersomes. A higher PC value corresponds to increased incorporation of the probe into the membrane. Therefore, VDG could favor the loss of packing of the head group of phospholipids.

On the other hand, Laurdan is useful to determine the phase state of the bilayer, because the GP function (for excitation and emission) acts as a fingerprint to discriminate among different membrane phase state scenarios [18]. The incorporation of the drug did not alter the phase state of the bilayers as expected after the results with MC540 (Figure 1). The curves corresponding to the GP spectra of excitation and emission are typical of a liquid-crystalline phase. Since the transition temperature between the gel and liquid-crystalline phase is around −20 °C for SPC, and the presence of VDG favored the loss of packing as observed with MC540, transfersomes continued to be in the liquid-crystalline phase after incorporation of the drug.

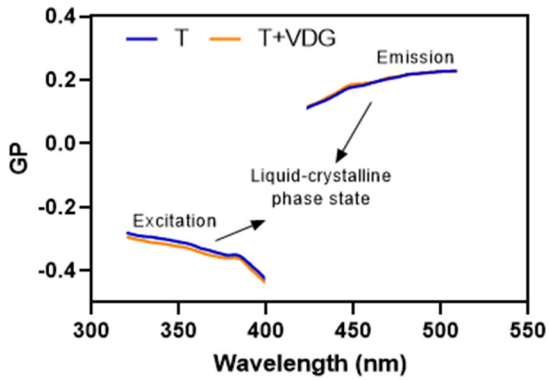


**Figure 1.** Laurdan excitation and emission GP spectra of empty transfersomes (T) and VDG-loaded transfersomes (T + VDG) at 25 °C. The curves consist of the averages of three independent measurements.

### 3.2. VDG Determination in Skin by UV-Visible Spectrophotometry

VDG was detected throughout all sections of the human and pig skin: shallow SC (1–5), medium SC (6–10), deep SC (11–20), and VED (Figure 2). Remarkably, while in the samples of human origin VDG were predominantly distributed in the first part of the SC, with a minor penetration percentage into the VED, in the pig skin samples, the opposite occurred, with a higher presence of the drug in the VED and lower retention in the SC.

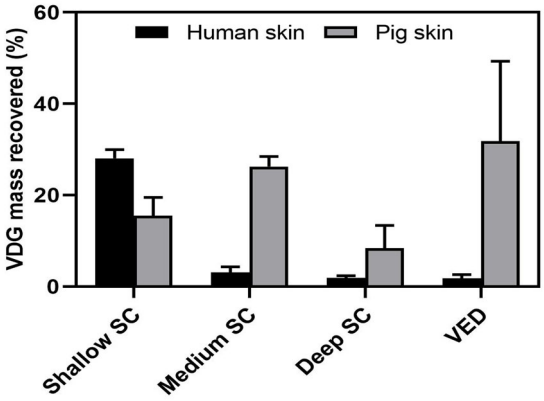


**Figure 2.** VDG recovered from the different sections of human and pig skin incubated with same amounts of T + VDG for 1 h at 35 °C ($n$ = 4). VDG was expressed as the percentage recovered from skin relative to the initial concentration of the incubated drug. Data are shown as mean ± SD.

While the literature generally validates the use of *ex vivo* porcine ear skin as a surrogate for human skin [19,20], our results, along with previous findings, draw attention to certain differences. A previous study regarding the penetration of fluorescently-labeled transfersomes in both human and pig skin [21] had shown some differences between these skin models for the penetration of this type of carrier, which was reaffirmed here with the profile of T + VDG. This is also consistent with observations made in previous studies [22], where in vivo human skin was compared to *ex vivo* pigskin at room temperature. In that case, higher permeability for pigskin to substances of different solubilities was noted. In this case, with both *ex vivo* samples incubated at body temperature, that trend is maintained. It is important to emphasize that the penetration of transfersomes depends on the existence of a moisture gradient in the skin. This should be taken into account regarding excipients that could be used in final formulations, as the literature shows how the Raman signal is affected at different depths of the skin by substances that can remove water, causing dehydration [23].

### 3.3. VDG Determination by Raman Spectroscopy

As can be seen in Figure 3, the Raman signals of the drug exhibited higher intensity in the superficial layers of the human SC than in the pig SC, and it showed partial agreement with the spectroscopic UV-visible assay. On the other hand, concerning the distribution of VDG in the VED shown in Figure 4, the Raman signals for both the carrier and the drug were detected more intensely in pig skin, whereas they were barely distinguishable from the background noise in the human samples. It was also coincident with the higher VDG signal in the UV-visible analysis for pig skin.

In Figures 3 and 4, the Raman spectra obtained from the different regions of human and pig skin are shown for empty transfersomes (T) and transfersomes loaded with VDG (T + VDG). In the cases detailed in the previous paragraph for Figure 4, a peak at 1434 $cm^{-1}$ corresponding to transfersomes, previously observed in the SC [24], was found. Additionally, a peak at 770 $cm^{-1}$ was observed in the VDG-loaded transfersomes in Figures 3 and 4, which coincides with a value previously reported through theoretical calculations [10]. Another peak reported for transfersomes at 1150 $cm^{-1}$ was also observed in pig VED, as well as other peaks corresponding to VDG at 350 $cm^{-1}$ and 415 $cm^{-1}$, were pointed out in

Figure 3. On the other hand, in Figure 5, a fourth derivative version of the Raman spectra of human skin in the VED is shown for better observation of the VDG presence, because the original signal presented very low intensity. Derivative analysis is commonly used to detect small signals hidden in the original spectra. Mathematically, if the original spectrum has a small peak (our case with the Raman Signal of VDG), the fourth derivative will put this in evidence. The first derivative of the original signal will be a line passing through zero, the second-order derivative will be an inverted peak with respect to the original signal. Finally, the fourth-order derivative is the inverse signal of the second-order derivative. This is the case of the Raman Spectra of VDG shown in Figure 5 [25]. In sum, these results could also confirm that VDG reaches the VED through this transport system.

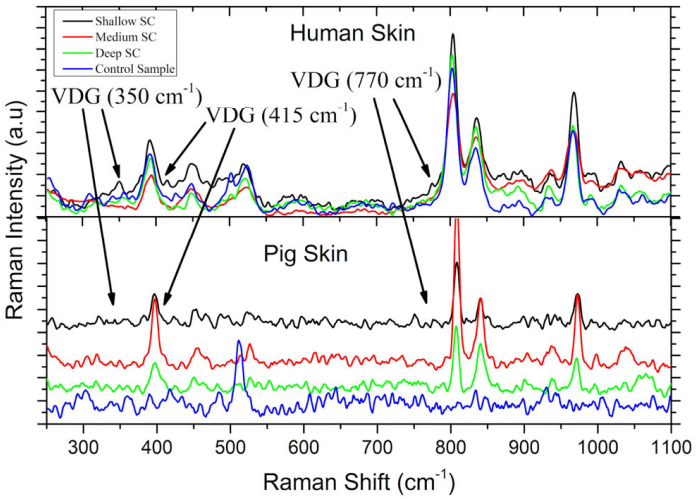


**Figure 3.** Raman spectra of tapes from tape stripping. In the upper part, the results from human skin samples are shown, while the lower part corresponds to pig skin samples. The controls were tapes stripped from untreated skin samples. Arrows show the peaks found corresponding to the VDG Raman signal.

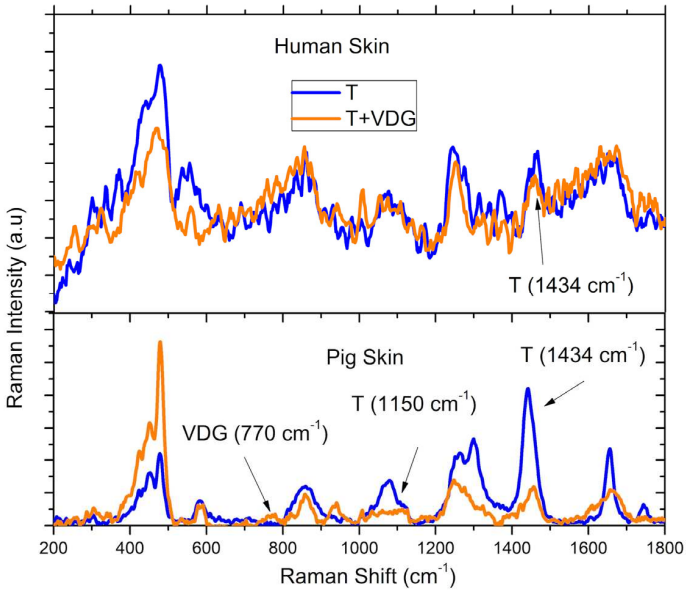


**Figure 4.** Raman spectra of VED from the remaining skin after tape stripping. The upper part shows the results from human skin samples, while the lower part corresponds to pig skin samples. In both cases, empty transfersomes (T) and VDG-loaded transfersomes (T + VDG) are shown. Arrows show the peaks found corresponding to the Raman signal of VDG, or from the lipid matrix of the transfersomes (T).

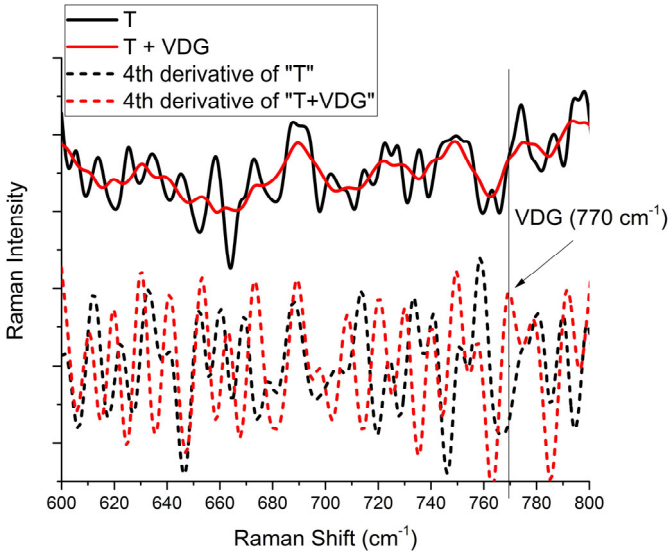


**Figure 5.** Enlarged version of the Raman spectra for T and T + VDG in VED of human skin in the region ranging from 600 to 800 $cm^{-1}$ and their fourth derivatives (in short dash), showing a slight shoulder at 770 $cm^{-1}$ attributable to the VDG signal.

### *3.4. Further Discussion*

UV-visible spectroscopy, whether using a conventional instrument or as part of an HPLC detector, has disadvantages for the measurement of VDG, due to its low absorbance and fluorescence. For these reasons, when using a UV-visible detector, organic extractions are necessary to obtain samples from the tapes, and grouping of these samples is required to obtain VDG concentrations that can be measurable by the detectors. On the other hand, when employing Raman, the acquisition of information is directly performed on the skin. In the context of diagnostic applications, and as a complement to therapeutic applications, the near-infrared wavelength used is harmless, with good skin penetration [26]. The acquisition mode is not only fast, but Raman detectors can also be constructed in a portable manner [27]. All these factors contribute to the significant biomedical potential of this method in relation to skin diseases.

The acquired Raman spectra allowed for the identification of active vibrational modes of the target species by comparing them with the spectra of solid VDG and transfersomes in aqueous suspension, obtained using a DXR Raman microscope [24]. A wavelength of 785 nm, corresponding to the near-infrared range, was chosen, utilizing 100% of its emission power (approximately 150 mW). This selection was made because many molecules exhibit sufficiently high fluorescence signals that can interfere and overlap with the Raman signal, especially in complex environments such as the skin, where melanin absorbs light in the visible range. In contrast, at this wavelength, there is a significant reduction in fluorescence intensity, allowing for efficient observation of Raman-active vibrational mode peaks [28]. On the other hand, the use of a grating with 600 grooves per mm implied a lower spectral resolution but a wider spectral range for scanning analysis. The peaks corresponding to the characteristic vibrational modes of transfersomes and VDG were previously described [24]. They were found at 1152 $cm^{-1}$ and 1437 $cm^{-1}$ for transfersomes, and at 350 $cm^{-1}$, 415 $cm^{-1}$, and 770 $cm^{-1}$ for VDG.

## 4. Conclusions

VDG, loaded into the membrane of liquid-crystalline transfersomes, can penetrate the skin; the detection of VDG and transfersomes signals indicates that the combination of SPM with Raman spectroscopy allowed for the detection of drug penetration in different layers of the skin. These tests demonstrate a correlation between the two techniques employed in this work, potentially enabling faster and direct detection by Raman, compared to

chromatography methods. Nevertheless, while Raman under these conditions would only allow for the detection of VDG presence, quantitative detection cannot be achieved by this method. This finding could be particularly valuable as a contributing complement to optimize dosages and assess the efficacy of potential future topical treatments.

**Author Contributions:** Conceptualization, J.M. and F.C.A.; methodology, G.E.G. and M.N.C.; software, M.N.C.; validation, G.E.G., J.M. and F.C.A.; formal analysis, G.E.G., M.N.C., J.M. and F.C.A.; investigation, G.E.G.; resources, S.d.V.A.; data curation, S.d.V.A.; writing—original draft preparation, G.E.G., J.M. and F.C.A.; writing—review and editing, J.M., M.N.C. and F.C.A.; visualization, M.N.C. and F.C.A.; supervision, J.M. and F.C.A.; project administration, J.M., F.C.A. and S.d.V.A.; funding acquisition, J.M., F.C.A. and S.d.V.A. All authors have read and agreed to the published version of the manuscript.

**Funding:** This research was funded by grants from Universidad Nacional de Quilmes, Universidad Nacional de Hurlingham, and CONICET (National Council of Scientific and Technical Research of Argentina).

**Institutional Review Board Statement:** The study was conducted in accordance with the Declaration of Helsinki and approved by the Ethics Committee of the National University of Quilmes (CE-UNQ N° 1/2019).

**Informed Consent Statement:** Informed consent was obtained from all subjects involved in the study.

**Data Availability Statement:** The data presented in this study are available on request from the corresponding author. The data are not publicly available due to privacy and ethicals.

**Acknowledgments:** This research has also been possible thanks to the economic contribution of Productos Roche S.A.Q. e I., Argentina. Calienni, Montanari, Alvira, and Alonso are members of CONICET, Argentina. Gómez acknowledges doctoral fellowship from Agencia I + D + i, Argentina.

**Conflicts of Interest:** The authors declare no conflict of interest.

## References

1. Sekulic, A.; Migden, M.R.; Oro, A.E.; Dirix, L.; Lewis, K.D.; Hainsworth, J.D.; Solomon, J.A.; Yoo, S.; Arron, S.T.; Friedlander, P.A.; et al. Efficacy and safety of Vismodegib in advanced basal-cell carcinoma. *N. Engl. J. Med.* **2012**, *366*, 2171–2179. [CrossRef] [PubMed]
2. Olesen, U.H.; Clergeaud, G.; Hendel, K.K.; Yeung, K.; Lerche, C.M.; Andresen, T.L.; Haedersdal, M. Enhanced and Sustained Cutaneous Delivery of Vismodegib by Ablative Fractional Laser and Microemulsion Formulation. *J. Investig. Dermatol.* **2020**, *140*, 2051–2059. [CrossRef] [PubMed]
3. Calienni, M.N.; Maza Vega, D.; Temprana, C.F.; Izquierdo, M.C.; Ybarra, D.E.; Bernabeu, E.; Moretton, M.; Alvira, F.C.; Chiappetta, D.; Alonso, S.D.V.; et al. The Topical Nanodelivery of Vismodegib Enhances Its Skin Penetration and Performance In Vitro While Reducing Its Toxicity *In Vivo*. *Pharmaceutics* **2021**, *13*, 186. [CrossRef] [PubMed]
4. Mishra, V.; Singh, M.; Mishra, Y.; Charbe, N.; Nayak, P.; Sudhakar, K.; Aljabali, A.A.A.; Shahcheraghi, S.H.; Bakshi, H.; Serrano-Aroca, Á.; et al. Nanoarchitectures in Management of Fungal Diseases: An Overview. *Appl. Sci.* **2021**, *11*, 7119. [CrossRef]
5. Lademann, J.; Jacobi, U.; Surber, C.; Weigmann, H.-J.; Fluhr, J.W. The tape stripping procedure—Evaluation of some critical parameters. *Eur. J. Pharm. Biopharm.* **2009**, *72*, 317–323. [CrossRef]
6. Smith, E.; Dent, G. *Modern Raman Spectroscopy: A Practical Approach*; John Wiley and Sons: Hoboken, NJ, USA, 2005; ISBN 0-471-49794-0.
7. Téllez S., C.A.; Costa, A.C., Jr.; Mondragón, M.A.; Ferreira, G.B.; Versiane, O.; Rangel, J.L.; Lima, G.M.; Martin, A.A. Molecular structure, natural bond analysis, vibrational and electronic spectra, surface enhanced Raman scattering and Mulliken atomic charges of the normal modes of $[Mn(DDTC)_2]$ complex. *Spectrochim. Acta A Mol. Biomol. Spectrosc.* **2016**, *169*, 95–107. [CrossRef]
8. Buckley, K.; Ryder, A.G. Applications of Raman Spectroscopy in Biopharmaceutical Manufacturing: A Short Review. *Appl. Spectrosc.* **2017**, *71*, 1085–1116. [CrossRef]
9. Franzen, L.; Selzer, D.; Fluhr, J.W.; Schaefer, U.F.; Windbergs, M. Towards drug quantification in human skin with confocal Raman microscopy. *Eur. J. Pharm. Biopharm.* **2013**, *84*, 437–444. [CrossRef]
10. Calienni, M.N.; Tuttolomondo, M.E.; Alonso, S.V.; Montanari, J.; Alvira, F.C. Experimental and theoretical study of the structural features of Vismodegib molecule. *J. Mol. Struct.* **2020**, *1205*, 127581. [CrossRef]
11. Ybarra, D.E.; Calienni, M.N.; Barraza Ramirez, L.F.; Aguayo Frias, E.T.; Lillo, C.; Alonso, S.; Montanari, J.; Alvira, F.C. Vismodegib in PAMAM-dendrimers for potential theragnosis in skin cancer. *Open Nano* **2022**, *7*, 100053. [CrossRef]

12. Calienni, M.N.; Febres-Molina, C.; Llovera, R.E.; Zevallos-Delgado, C.; Tuttolomondo, M.E.; Paolino, D.; Fresta, M.; Barazorda-Ccahuana, H.L.; Gómez, B.; del Valle Alonso, S.; et al. Nanoformulation for potential topical delivery of Vismodegib in skin cancer treatment. *Int. J. Pharm.* **2019**, *565*, 108–122. [CrossRef]
13. Marsanasco, M.; Márquez, A.L.; Wagner, J.R.; Chiaramoni, N.S.; Alonso, S.V. Bioactive compounds as functional food ingredients: Characterization in model system and sensory evaluation in chocolate milk. *J. Food Eng.* **2015**, *166*, 55–63. [CrossRef]
14. Parasassi, T.; Gratton, E. Membrane lipid domains and dynamics as detected by Laurdan fluorescence. *J. Fluoresc.* **1995**, *5*, 59–69. [CrossRef] [PubMed]
15. Stewart, J.C.M. Colorimetric determination of phospholipids with ammonium ferrothiocyanate. *Anal. Biochem.* **1980**, *104*, 10–14. [CrossRef] [PubMed]
16. Disalvo, E.A.; Arroyo, J.; Bernik, D.L. Interfacial properties of liposomes as measured by fluorescence and optical probes. *Methods Enzymol.* **2003**, *367*, 213–233. [CrossRef]
17. Lelkes, P.I.; Miller, I.R. Perturbations of membrane structure by optical probes: I. Location and structural sensitivity of merocyanine 540 bound to phospholipid membranes. *J. Membr. Biol.* **1980**, *52*, 1–15. [CrossRef]
18. Bagatolli, L.A. LAURDAN Fluorescence Properties in Membranes: A Journey from the Fluorometer to the Microscope. In *Fluorescent Methods to Study Biological Membranes. Springer Series on Fluorescence*; Mély, Y., Duportail, G., Eds.; Springer: Berlin/Heidelberg, Germany, 2012; Volume 13. [CrossRef]
19. Sgorbini, B.; Cagliero, C.; Argenziano, M.; Cavalli, R.; Bicchi, C.; Rubiolo, P. In vitro release and permeation kinetics of *Melaleuca alternifolia* (tea tree) essential oil bioactive compounds from topical formulations. *Flavour. Fragr. J.* **2017**, *32*, 354–361. [CrossRef]
20. Soto, F.; Jeerapan, I.; Silva-López, C.; Lopez-Ramirez, M.A.; Chai, I.; Xiaolong, L.; Lv, J.; Kurniawan, J.F.; Martin, I.; Chakravarthy, K.; et al. Noninvasive transdermal delivery system of lidocaine using an acoustic droplet-vaporization based wearable patch. *Small* **2018**, *14*, 1803266. [CrossRef]
21. Izquierdo, M.C.; Lillo, C.R.; Bucci, P.; Gomez, G.E.; Martínez, L.; Alonso, S.D.V.; Calienni, M.N.; Montanari, J. Comparative skin penetration profiles of formulations including ultradeformable liposomes as potential nanocosmeceutical carriers. *J. Cosmet. Dermatol.* **2020**, *19*, 3127–3137. [CrossRef]
22. Choe, C.; Schleusener, J.; Lademann, J.; Darvin, M.E. Human skin in vivo has a higher skin barrier function than porcine skin ex vivo-comprehensive Raman microscopic study of the stratum corneum. *J. Biophotonics* **2018**, *11*, e201700355. [CrossRef]
23. Sdobnov, A.Y.; Darvin, M.E.; Schleusener, J.; Lademann, J.; Tuchin, V.V. Hydrogen bound water profiles in the skin influenced by optical clearing molecular agents-Quantitative analysis using confocal Raman microscopy. *J. Biophotonics* **2019**, *12*, e201800283. [CrossRef] [PubMed]
24. Calienni, M.N.; Montanari, J.; Tuttolomondo, M.E.; Gomez, G.; Alonso, S.V.; Alvira, F.C. Raman spectroscopy study of a topical penetration of a new generation skin-cancer antineoplastic drug. In *Latin America Optics and Photonics Conference*; Paper Tu3C.5; OSA Technical Digest (Optica Publishing Group): Washington, DC, USA, 2018. [CrossRef]
25. Redasani, V.K.; Patel, P.R.; Marathe, D.Y.; Chaudhari, S.R.; Shirkhedkar, A.A.; Surana, S.J. A review on derivative uv-spectrophotometry analysis of drugs in pharmaceutical formulations and biological samples review. *J. Chil. Chem. Soc.* **2018**, *63*, 4126–4134. [CrossRef]
26. Liu, Y.; Lunter, D.J. Confocal Raman spectroscopy at different laser wavelengths in analyzing stratum corneum and skin penetration properties of mixed PEGylated emulsifier systems. *Int. J. Pharm.* **2022**, *616*, 121561. [CrossRef]
27. Lin, Q.; Lazareva, E.N.; Kochubey, V.I.; Duan, Y.; Tuchin, V.V. Kinetics of optical clearing of human skin studied in vivo using portable Raman spectroscopy. *Laser Phys. Lett.* **2020**, *17*, 10. [CrossRef]
28. Tfaili, S.; Gobinet, C.; Josse, G.; Angiboust, J.F.; Manfait, M.; Piot, O. Confocal Raman microspectroscopy for skin characterization: A comparative study between human skin and pig skin. *Analyst* **2012**, *137*, 3673–3682. [CrossRef]